Magnon-squeezing-enhanced slow light and second-order sideband in cavity magnomechanics

Tian-Xiang Lu,[1] Xing Xiao,[1] Liu-Sha Chen,[1] Qian Zhang,[2] and Hui Jing[2,3,*]

[1]*College of Physics and Electronic Information, Gannan Normal University, Ganzhou 341000, Jiangxi, China*

[2]*Key Laboratory of Low-Dimensional Quantum Structures and Quantum Control of Ministry of Education, Department of Physics and Synergetic Innovation Center for Quantum Effects and Applications, Hunan Normal University, Changsha 410081, China*

[3]*Synergetic Innovation Academy for Quantum Science and Technology, Zhengzhou University of Light Industry, Zhengzhou 450002, China*

(Received 18 October 2022; revised 9 May 2023; accepted 12 June 2023; published 29 June 2023)

Cavity magnomechanics (CMM) has rapidly become a new research field of cavity quantum electrodynamics for studying quantum information processing and sensing. Here, we theoretically study the magnomechanically induced transparency effect in a cavity magnomechanical system, focusing on the role of magnon squeezing in enhancing and controlling the group delay of the transmitted light. As a result, we find that the magnon number can be strongly affected by magnon squeezing, accompanied by a steerable transmission rate and controllable fast-to-slow light switching. In particular, in the photon-magnon strong-coupling scenario, the group delay of the probe field can be enhanced by about three times by using magnon squeezing compared to the case without magnon squeezing. Moreover, due to the presence of magnon squeezing, the efficiency of the second-order sideband in the photon-magnon weak-coupling scenario can also be enhanced compared to the case without magnon squeezing. These results provide tools to engineer CMM devices with magnon squeezing for, e.g., light propagation and storage, and precision measurements of weak signals.

DOI: 10.1103/PhysRevA.107.063714

I. INTRODUCTION

Hybrid quantum systems hold the potential to build quantum networks with complementary properties in existing quantum technologies, especially in quantum computing, quantum communication, and quantum sensing [1]. A new class of hybrid systems is hybrid magnonic devices based on collective spin excitations of an yttrium iron garnet (YIG) sphere with high spin density, strong spin-spin exchange interactions, and a relatively low damping rate, that build a platform to bridge an optical field with the magnetic systems [2–8]. In such devices, by coupling the magnons (the collective spin excitations in YIG) with microwave or optical photons [9–19], promising applications are actively explored, such as long-time memory [20,21], spin current control [22,23], coherent optical-to-microwave conversion [24–26], magnon and photon manipulating using exceptional points [27–37], quantum entanglement of magnons [38,39], magnon-induced nonreciprocity [40,41], precision measurements [42–45], etc.

In parallel, the magnons can also couple to deformation vibration phonons through magnetostrictive force [46–49], known as cavity magnomechanics (CMM), to explore many intriguing applications, i.e., magnon-phonon entanglement and magnon-squeezing states [50–58], ultraslow light engineering [59–61], magnon laser or chaos [62–64], a magnetometer or thermometer [65,66], ground-state cooling of the mechanical vibration mode [67–70], photon-phonon interface [71,72], and quantum state storage and retrieval [73], to mention a few examples. At the same time, we note that, by utilizing the squeezing of the magnon mode, the ground-state cooling [74] and entanglement [75] can be enhanced in the CMM system. Squeezed states [76], an important quantum state, play an important role in quantum precision measurement and quantum information processing. For example, squeezed light can be used to improve the sensitivity of interferometers for gravitational-wave detection [77,78], produce an entangled source for quantum teleportation [79], and explore the quantum and classical borderline [80], among many others. Inspired by these superior characteristics, various approaches have been proposed to generate squeezed states of the photons and magnons based on the CMM system, such as using the anisotropy of the ferromagnet [3], applying the two-tone microwave fields to drive the magnon mode [58], promising a wide range of applications on improving the sensitivity of position measurement [81] and magnetic resonance spectroscopy [82].

In this paper, we consider a CMM system with magnon squeezing to study magnomechanically induced transparency (MMIT) effects, including the signal transmission, group delay, and its higher-order sidebands. We show that the magnon-squeezing parameter and the phase lead to the enhancement and periodic variation of the magnon number, endowing the MMIT with unconventional features. That is, the transmission rate and the width of the transparency window can be adjusted by tuning the squeezing parameter and phase. Particularly, we find that the group delay of the transmitted light has distinct characteristics for different photon-magnon coupling cases, i.e., (i) in the photon-magnon strong-coupling (PMSC) scenario, controllable slow-to-fast light switching and about a threefold enhancement of the

*jinghui73@gmail.com

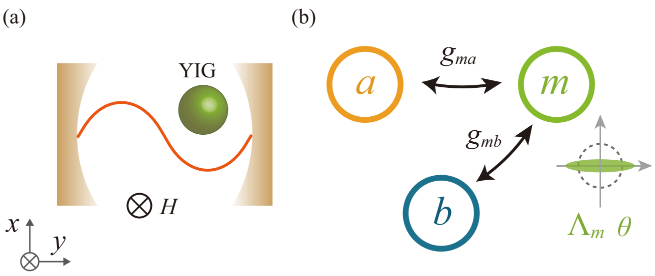

FIG. 1. (a) Schematic illustration of the CMM system composed of a microwave cavity with a highly polished YIG sphere. The YIG sphere, supporting a magnon mode m and a phonon mode b [46,47], is placed in a cavity such that it is simultaneously near the maximum magnetic field of the cavity mode a and in a uniform bias magnetic field along the z axis, which is responsible for magnon-photon coupling. Magnon-phonon coupling also can be realized via the magnetostrictive interaction. (b) Schematic of the equivalent mode-coupling model. g_{ma} or g_{mb} is the photon-magnon coupling strength or the magnon-phonon coupling strength, respectively. The green ellipse represents the squeezing of the magnon mode with the squeezing parameter Λ_m and the phase θ, which can be used to enhance slow light and high-order sidebands.

group delay of the probe field compared to the case without the magnon squeezing can be achieved, which is not attainable in the photon-magnon weak-coupling (PMWC) scenario; (ii) in contrast to the PMSC scenario, the group delay of the second-order sideband experiences a transition from advance to delay and enhancement only in the case of PMWC; (iii) in the PMWC scenario, the efficiency of the second-order sideband can also be improved due to the presence of magnon squeezing. These features show that CMM devices with magnon squeezing can serve as powerful tools for manipulating photons and phonons, with potential applications in optical signal storage and communications [59–61,83], even in quantum metrology [65,66,78].

II. THEORETICAL MODEL

As shown in Fig. 1, we consider a single-mode microwave cavity of resonance frequency ω_a and damping rate κ_a, coupled with a highly polished YIG sphere. The YIG sphere glued to the end of a silica fiber is placing in the cavity near the maximum magnetic field of the cavity mode [9–19]. Simultaneously, an external magnetic field H is applied in the z direction, and a uniform magnon mode with damping rate κ_m appears in the sphere at the resonance frequency $\omega_m = \gamma H$, where $\gamma = 2\pi \times 28$ GHz/T is the gyromagnetic ratio. The magnon and photon modes are strongly coupled to each other via a magnetic dipole interaction, which has been demonstrated experimentally [9–19]. According to Ref. [11], by scaling down the cavity size and increasing the number of spins, the obtained coupling strength and the damping rates of the photon and the magnon are $g_{ma}/2\pi = 10.8$ MHz, $\kappa_{ma}/2\pi = 1.35$ MHz, and $\kappa_{ma}/2\pi = 1.06$ MHz, respectively, deep in the strong-coupling regime with a cooperativity of $C = 81$ ($C = g_{ma}^2/\kappa_a\kappa_m \gg 1$). In addition, the YIG sphere can also support a mechanical vibration mode (phonon) with frequency ω_b and damping rate γ_b [46–49], and magnon-phonon coupling can be realized by a magnetostrictive interaction. Here, the radiation pressure optomechanical interaction can be fully neglected due to the smaller size of the YIG sphere (10^2 µm–1 mm) compared to the wavelength of the microwave field.

In a frame rotating at the pump frequency ω_l, with a weak probe field of the frequency ω_p and the amplitudes ε_p, the total Hamiltonian of this system can be written as ($\hbar = 1$)

$$\begin{aligned}
\mathcal{H} &= \mathcal{H}_0 + \mathcal{H}_{\rm int} + \mathcal{H}_{\rm dr},\\
\mathcal{H}_0 &= \Delta_a a^\dagger a + \Delta_m m^\dagger m + \omega_b b^\dagger b,\\
\mathcal{H}_{\rm int} &= g_{ma}(a^\dagger m + m^\dagger a) + g_{mb} m^\dagger m(b + b^\dagger),\\
\mathcal{H}_{\rm dr} &= i\varepsilon_l m^\dagger + i\varepsilon_p e^{-i\xi t} a^\dagger + \frac{i}{2}\Lambda_m m^{\dagger 2} e^{i\theta} - \text{H.c.},
\end{aligned} \tag{1}$$

where $\Delta_a = \omega_a - \omega_l$, $\Delta_m = \omega_m - \omega_l$, and $\xi = \omega_p - \omega_l$. a ($a^\dagger$), m ($m^\dagger$), and b ($b^\dagger$) are the annihilation (creation) operators of the cavity, magnon, and the phonon mode, respectively. g_{ma} or g_{mb} denotes the magnon-photon or magnon-phonon coupling coefficient. $\varepsilon_l = \gamma\sqrt{5N}B_0/4$ is the drive strength with the field amplitude B_0, the frequency ω_0, and the total number of spins $N = \rho V$, with $\rho = 4.22 \times 10^{27}$ m^{-3} (ρ is the spin density and V is the volume of the sphere) [50–52]. Here, this term $\Lambda_m m^{\dagger 2} e^{i\theta}/2 - \text{H.c.}$ in the Hamiltonian represents the squeezing of the magnon mode with the squeezing parameter Λ_m and the phase θ, which can be realized by, e.g., transferring squeezing from the cavity with a squeezed vacuum field [57], or applying the two-tone microwave fields to drive the magnon mode [58], or using the anisotropy of the ferromagnet [3,84], or the intrinsic nonlinearity of the magnetostriction [85], or driving the qubit with two microwave fields in cavity-magnon-qubit systems [86]. For instance, Li *et al.* theoretically demonstrated the existence of magnon squeezed states and that squeezing of magnons by about 5.40 dB can be achieved for $g_{ma}/2\pi = 20$ MHz [57]. In the following, we focus on the features of MMIT by exploiting the squeezing of the magnon mode, including the signal transmission, group delay, and its higher-order sidebands.

Similarly to previous optomechanically induced transparency works in cavity optomechanical systems [87–89], MMIT only deals with the mean response of the system to the probe field without including quantum fluctuation [46]. Therefore, in order to explore the nonlinear dynamics of the system, we employ the Heisenberg-Langevin equations and reduce operators to their expectation values [i.e., $o(t) = \langle \hat{o(t)} \rangle$ ($o = a, m, b$)]. Then the Heisenberg-Langevin equations of this system are

$$\begin{aligned}
\dot{m} &= -[i\Delta_m + \kappa_m + ig_{mb}(b + b^\dagger)]m\\
&\quad - ig_{ma}a + \varepsilon_l + \Lambda_m m^\dagger e^{i\theta},\\
\dot{a} &= -(i\Delta_a + \kappa_a)a - ig_{ma}m + \varepsilon_p e^{-i\xi t},\\
\dot{b} &= -(i\omega_b + \gamma_b)b - ig_{mb}m^\dagger m.
\end{aligned} \tag{2}$$

For the case where the probe field in MMIT typically is much weaker than the pump field [46,87], we can expand every operator as the sum of its steady-state value and a small fluctuation (perturbation method) [90] to deal with Eqs. (2),

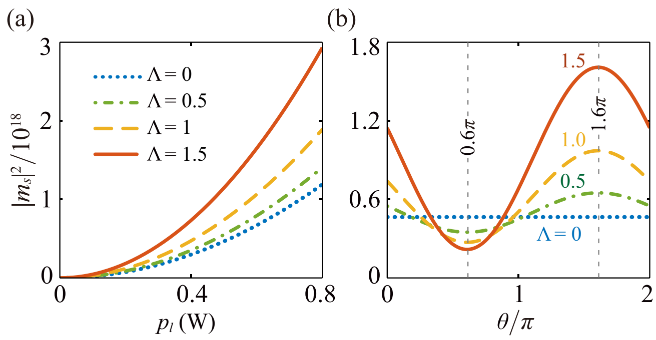

FIG. 2. (a) Numerical solutions of Eq. (4). (a) For $\theta = 0$, mean magnon number $|m_s|^2$ is plotted as a function of the drive power p_l for different $\Lambda = \Lambda_m/\kappa_a$. (b) For $p_l = 0.5$ W, corresponding to the drive strength $\varepsilon_l \simeq 2\times 10^{17}$ Hz, $|m_s|^2$ is plotted as a function of the phase θ for different Λ. We choose $g_{ma} = 0.9\kappa_a$ in (a) and (b) and the other parameters can be found in the main text.

i.e., $o = o_s + \delta o$. The pump field provides a steady-state solution of the system, while the probe field is treated as the perturbation of the steady state. Then we have the steady-state values

$$m_s = \frac{(\Lambda_m m_s^* e^{i\theta} + \varepsilon_l)(i\Delta_a + \kappa_a)}{(i\Delta_s + \kappa_m)(i\Delta_a + \kappa_a) + g_{ma}^2},$$
$$a_s = \frac{-ig_{ma} m_s}{i\Delta_a + \kappa_a}, \quad b_s = \frac{-ig_{mb}|m_s|^2}{i\omega_b + \gamma_b}. \tag{3}$$

where $\Delta_s = \Delta_m + 2g_{mb}\,\mathrm{Re}(b_s)$ including the magnomechanically induced frequency shift. Compared to the detuning term Δ_m, the term $2g_{mb}\,\mathrm{Re}(b_s)$ is small due to the fact that g_{mb} is typically small (3–60 mHz) [46–49]. i.e., $|\Delta_s - \Delta_m| \ll \Delta_m$. In order to study more clearly the effect of magnon squeezing on the mean magnon number, for simplicity, we take $\Delta_s \simeq \Delta_m$ in Eqs. (3). Then it is straightforward to show that m_s satisfies

$$m_s = \frac{(\Delta_a^2 + \kappa_a^2)\Lambda_m e^{i\theta} + (i\Delta_a + \kappa_a)\mathcal{L}}{|\mathcal{L}|^2 - (\Delta_a^2 + \kappa_a^2)\Lambda_m^2}\varepsilon_l, \tag{4}$$

where $\mathcal{L} = (-i\Delta_m + \kappa_m)(-i\Delta_a + \kappa_a) + g_{ma}^2$. The mean magnon number $|m_s|^2$, being related to both the squeezing parameter Λ and the phase θ, is shown in Fig. 2 for the PMWC scenario ($g_{ma} = 0.9\kappa_a$). For $\theta = 0$, $|m_s|^2$ can be enhanced by increasing the squeezing parameter Λ [see Fig. 2(a)]. For a fixed Λ, the phase θ changes can increase or decrease the magnon number [see Fig. 2(b)], which in turn can significantly modify the linear and nonlinear MMIT process. By solving Eq. (4) analytically, for $\theta \simeq 0.6\pi$, we have the smallest mean magnon number, while for $\theta \simeq 1.6\pi$, we have the largest mean magnon number at a fixed Λ. In the PMSC scenario ($g_{ma} = 2\kappa_a$), the mean magnon number $|m_s|^2$ with respect to the squeezing parameter and phase has a similar variation curve as in Fig. 2 and is not shown.

Now we consider the perturbation induced by the input probe field. After eliminating the steady-state values, Eqs. (2) become

$$\begin{aligned}
\delta\dot{m} &= -(i\Delta_s + \kappa_m)\delta m - ig_{mb}m_s(\delta b + \delta b^\dagger)\\
&\quad - ig_{mb}(\delta b + \delta b^\dagger)\delta m - ig_{ma}\delta a + \Lambda_m e^{i\theta}\delta m^\dagger,\\
\delta\dot{a} &= -(i\Delta_a + \kappa_a)\delta a - ig_{ma}\delta m + \varepsilon_p e^{-i\xi t},\\
\delta\dot{b} &= -(i\omega_b + \gamma_b)\delta b - ig_{mb}(m_s^*\delta m + m_s\delta m^\dagger + \delta m^\dagger\delta m).
\end{aligned} \tag{5}$$

To calculate the amplitudes of the first- and second-order sidebands of inputting a probe field, we using the following ansatz [46,87]:

$$\begin{aligned}
\delta m &= \mathcal{M}_1^- e^{-i\xi t} + \mathcal{M}_1^+ e^{i\xi t} + \mathcal{M}_2^- e^{-2i\xi t} + \mathcal{M}_2^+ e^{2i\xi t} + \cdots,\\
\delta a &= \mathcal{A}_1^- e^{-i\xi t} + \mathcal{A}_1^+ e^{i\xi t} + \mathcal{A}_2^- e^{-2i\xi t} + \mathcal{A}_2^+ e^{2i\xi t} + \cdots,\\
\delta b &= \mathcal{B}_1^- e^{-i\xi t} + \mathcal{B}_1^+ e^{i\xi t} + \mathcal{B}_2^- e^{-2i\xi t} + \mathcal{B}_2^+ e^{2i\xi t} + \cdots.
\end{aligned} \tag{6}$$

The physical picture of such an ansatz is that there are output fields with frequencies $\omega_l \pm n\xi$ generated in such a CMM system [59,91], due to the nonlinear terms $-ig_{mb}(\delta b + \delta b^\dagger)\delta m$ and $-ig_{mb}\delta m^\dagger\delta m$ in Eq. (5), where n is an integer. In the present work, we only consider the first- and second-order sidebands, and the higher-order sidebands are ignored. Therefore, substituting Eq. (6) into Eq. (5) leads to 12 algebraic equations, which can be simplified into two groups because the second-order sideband is a second-order process whose amplitude is much smaller than the probe field [91]: One group describes the linear response,

$$\begin{aligned}
\alpha_1^+\mathcal{A}_1^- &= -ig_{ma}\mathcal{M}_1^- + \varepsilon_P, \quad \alpha_1^-\mathcal{A}_1^{+*} = ig_{ma}\mathcal{M}_1^{+*},\\
\beta_1^+\mathcal{M}_1^- &= -ig_{ma}\mathcal{A}_1^- - iG(\mathcal{B}_1^{+*} + \mathcal{B}_1^-) + \Lambda_m e^{i\theta}\mathcal{M}_1^{+*},\\
\beta_1^-\mathcal{M}_1^{+*} &= ig_{ma}\mathcal{A}_1^{+*} + iG^*(\mathcal{B}_1^{+*} + \mathcal{B}_1^-) + \Lambda_m e^{-i\theta}\mathcal{M}_1^-,\\
\gamma_1^+\mathcal{B}_1^- &= -iG^*\mathcal{M}_1^- - iG\mathcal{M}_1^{+*},\\
\gamma_1^-\mathcal{B}_1^{+*} &= iG\mathcal{M}_1^{+*} + iG^*\mathcal{M}_1^-,
\end{aligned} \tag{7}$$

and the other group describes the second-order sideband,

$$\begin{aligned}
\alpha_2^+\mathcal{A}_2^- &= -ig_{ma}\mathcal{M}_2^-, \quad \alpha_2^-\mathcal{A}_2^{+*} = ig_{ma}\mathcal{M}_2^{+*},\\
\gamma_2^+\mathcal{B}_2^- &= -iG^*\mathcal{M}_2^- - iG\mathcal{M}_2^{+*} - ig_{mb}\mathcal{M}_1^-\mathcal{M}_1^{+*},\\
\gamma_2^-\mathcal{B}_2^{+*} &= iG\mathcal{M}_2^{+*} + iG^*\mathcal{M}_2^- + ig_{mb}\mathcal{M}_1^{+*}\mathcal{M}_1^-,\\
\beta_2^+\mathcal{M}_2^- &= -ig_{ma}\mathcal{A}_2^- - iG(\mathcal{B}_2^- + \mathcal{B}_2^{+*}) + \Lambda_m e^{i\theta}\mathcal{M}_2^{+*}\\
&\quad - ig_{mb}\mathcal{M}_1^-(\mathcal{B}_1^- + \mathcal{B}_1^{+*}),\\
\beta_2^-\mathcal{M}_2^{+*} &= ig_{ma}\mathcal{A}_2^{+*} + iG^*(\mathcal{B}_2^{+*} + \mathcal{B}_2^-) + \Lambda_m e^{-i\theta}\mathcal{M}_2^-\\
&\quad + ig_{mb}\mathcal{M}_1^{+*}(\mathcal{B}_1^{+*} + \mathcal{B}_1^-),
\end{aligned} \tag{8}$$

where $G = g_{mb}m_s$, and

$$\begin{aligned}
\alpha_1^\pm &= -i\xi \pm i\Delta_a + \kappa_a, \quad \alpha_2^\pm = -2i\xi \pm i\Delta_a + \kappa_a,\\
\beta_1^\pm &= -i\xi \pm i\Delta_s + \kappa_m, \quad \beta_2^\pm = -2i\xi \pm i\Delta_s + \kappa_m,\\
\gamma_1^\pm &= -i\xi \pm i\omega_b + \gamma_b, \quad \gamma_2^\pm = -2i\xi \pm i\omega_b + \gamma_b.
\end{aligned}$$

Solving Eqs. (7) and (8) leads to

$$\mathcal{A}_1^- = \frac{(\mathcal{K}+\mathcal{V}_1+\mathcal{D}_1)\varepsilon_p}{\alpha_1^+(\mathcal{V}_1+\mathcal{D}_1)+\mathcal{Q}_1+4\omega_b\Delta_a|G|^2g_{ma}^2},$$
$$\mathcal{M}_1^{+*} = \frac{-ig_{ma}\alpha_1^-\varepsilon_P(\gamma_1^+\gamma_1^-\Lambda_m e^{-i\theta}-2iG^{*2}\omega_b)}{\alpha_1^+(\mathcal{V}_1+\mathcal{D}_1)+\mathcal{Q}_1+4\omega_b\Delta_a|G|^2g_{ma}^2},$$
$$\mathcal{M}_1^- = \frac{-ig_{ma}\varepsilon_P\big[\gamma_1^+\gamma_1^-\big(\alpha_1^-\beta_1^-+g_{ma}^2\big)+2i|G|^2\omega_b\alpha_1^-\big]}{\alpha_1^+(\mathcal{V}_1+\mathcal{D}_1)+\mathcal{Q}_1+4\omega_b\Delta_a|G|^2g_{ma}^2},$$
$$\mathcal{A}_2^- = \frac{2g_{ma}g_{mb}\omega_b(\mathcal{P}_1-\mathcal{P}_2+\mathcal{P}_3)}{\gamma_1^+\gamma_1^-\big[\alpha_2^+(\mathcal{V}_2+\mathcal{D}_2)+\mathcal{Q}_2+4\omega_b\Delta_a|G|^2g_{ma}^2\big]}, \quad (9)$$

where $\mathcal{K}=g_{ma}^2(\beta_1^+\gamma_1^+\gamma_1^- - 2i\omega_b|G|^2)$, and

$$\mathcal{V}_j = \alpha_j^-\beta_j^+\beta_j^-\gamma_j^+\gamma_j^- - 4\alpha_j^-\omega_b\Delta_s|G|^2,$$
$$\mathcal{Q}_j = \gamma_j^+\gamma_j^-\big(\alpha_j^+\beta_j^+g_{ma}^2+\alpha_j^-\beta_j^-g_{ma}^2+g_{ma}^4\big),$$
$$\mathcal{D}_j = 2i\omega_b\alpha_j^-\Lambda_m(G^{*2}e^{i\theta}-G^2e^{-i\theta})-\Lambda_m^2\alpha_j^-\gamma_j^+\gamma_j^-,$$
$$\mathcal{P}_1 = 2i\omega_b\alpha_2^-\big(|G|^2G^*\mathcal{M}_1^{-2}-G^3\mathcal{M}_1^{+*2}\big),$$
$$\mathcal{P}_2 = \alpha_2^-\Lambda_m e^{i\theta}\big(\gamma_2^+\gamma_2^-G\mathcal{M}_1^{+*2}+G^*\mathcal{I}\mathcal{M}_1^-\mathcal{M}_1^{+*}\big),$$
$$\mathcal{P}_3 = \big(\alpha_2^-\beta_2^-+g_{ma}^2\big)\big(\gamma_2^+\gamma_2^-G^*\mathcal{M}_1^{-2}+G\mathcal{I}\mathcal{M}_1^-\mathcal{M}_1^{+*}\big),$$

where $j=1,2$ and $\mathcal{I}=\gamma_1^+\gamma_1^-+\gamma_2^+\gamma_2^-$. $\mathcal{A}_1^-$ and $\mathcal{A}_2^-$ are the coefficients of the first- and second-order upper sidebands, respectively. By using the standard input-output relations [92], i.e., $a_{\text{out}}=a_{\text{in}}-\sqrt{2\kappa_a}a(t)$, where a_{in} (a_{out}) is the input (output) probe operators, we can obtain the expectation value

$$\langle a_{\text{out}}\rangle = s_0e^{-i\omega_l t}+s_1e^{-i\omega_p t}-\sqrt{2\kappa_a}\mathcal{A}_2^-e^{-i(2\omega_p-\omega_l)t} - \sqrt{2\kappa_a}\mathcal{A}_1^+e^{-i(2\omega_l-\omega_p)t}-\sqrt{2\kappa_a}\mathcal{A}_2^+e^{-i(3\omega_l-2\omega_p)t}, \quad (10)$$

with $s_0=\varepsilon_l/\sqrt{2\kappa_a}-\sqrt{2\kappa_a}a_s$ and $s_1=\varepsilon_p/\sqrt{2\kappa_a}-\sqrt{2\kappa_a}\mathcal{A}_1^-$, where $s_0e^{-i\omega_l t}$ or $s_1e^{-i\omega_p t}$ denote the output fields with a pump frequency ω_l or ω_p, respectively, while the term $-\sqrt{2\kappa_a}\mathcal{A}_1^+e^{-i(2\omega_l-\omega_p)t}$ describes the Stokes process, respectively. Moreover, the terms $\sqrt{2\kappa_a}\mathcal{A}_2^+e^{-i(3\omega_l-2\omega_p)t}$ and $-\sqrt{2\kappa_a}\mathcal{A}_2^-e^{-i(2\omega_p-\omega_l)t}$, describing the output with frequencies $\omega_l\pm 2\xi$, are related to the second-order upper and lower sideband process [59,91]. Hence, the transmission rate of the probe field or the efficiency of the second-order upper sideband can be written as [91]

$$T=|t_p|^2=\left|1-\frac{2\kappa_a}{\varepsilon_p}\mathcal{A}_1^-\right|^2, \quad \eta=\left|-\frac{2\kappa_a}{\varepsilon_p}\mathcal{A}_2^-\right|. \quad (11)$$

It is obvious that η is proportional to $\mathcal{A}_2^-$, and we note that $\mathcal{A}_2^-$ consists of three parts: The second-order sideband terms based on nonlinear magnetostrictive interaction, the upconverted first-order sideband terms, and the magnon-squeezing terms. This implies that, besides the nonlinear magnetostrictive interaction and the upconverted process of the first-order sideband [91], the second-order sideband can also be steered by tuning the squeezing parameter. With this at hand, we can discuss the effect of magnon squeezing on MMIT.

III. RESULTS AND DISCUSSION

A. Linear MMIT spectrum and group delay

In numerical simulations, to demonstrate that the observation of the MMIT process is within current experimental reach, we have selected experimentally feasible parameters [46–49], i.e., $\omega_a/2\pi=\omega_m/2\pi=13.205$ GHz, $\kappa_a/2\pi=15$ MHz, $\kappa_m/2\pi=15$ MHz, $\omega_b/2\pi=50$ MHz, $\gamma_b/2\pi=200$ kHz, and $g_{mb}/\pi=9.9$ mHz, $\varepsilon_P/\varepsilon_l=0.05$, $\Delta_a=\Delta_m=\omega_b$, respectively.

In Fig. 3, the transmission rate T is shown as a function of the probe detuning $\Delta_p/\omega_b=(\xi-\omega_b)/\omega_b$ and the phase θ. For comparisons, we first consider the case without magnon squeezing. In the PMWC coupling scenario, we chose $g_{ma}=0.9\kappa_a$, such that an asymmetric Lorentzian-shaped transparency window of MMIT appears around the resonance point $\Delta_p=0$ [see the blue dashed curve in Fig. 3(a)], as a result of the phonon-induced resonances effect [46]. In the PMSC scenario, we take $g_{ma}=2\kappa_a$, for example. Double transparency windows appear in the transmission spectra [see the blue dashed curve in Fig. 3(d)], due to the presence of the phonon mode which splits the original magnetically induced transparency peak into two [11,70].

If magnon squeezing is present, i.e., $\Lambda=1.5$ and $\theta=0$, a wider transparency window and a higher transmission rate at the resonance point can be obtained for the PMWC scenario [see the red solid curve in Fig. 3(a)]. The reason is that the increase in magnon number caused by magnon squeezing [see Fig. 2(a)] leads to a wide MMIT window [87], i.e., the linewidth of the MMIT window is related to the magnon number,

$$\Gamma=\gamma_b+\frac{g_{mb}^2|m_s|^2}{\kappa_m}. \quad (12)$$

We also obtain a similar performance in the PMSC scenario [see the red solid curve in Fig. 3(d)]. The slight difference is that in the PMSC scenario, the transmission spectrum near the resonance point changes from absorption to transparency rather than simple amplification. In addition, more interesting phenomena can be observed by tuning the phase. Figures 3(b) and 3(e) show the transmission rate with different phases θ at a fixed $\Lambda=1.5$. The phase of the magnon squeezing affects the magnon number on a regular basis [see Fig. 2(b)], Â so that the linewidth of the transparency window and the transmission rate are also regularly affected. For $\theta=0.6\pi$, strong absorption of the probe light can be achieved, while for $\theta=1.6\pi$, we can obtain the maximum transmission rate [see Figs. 3(c) and 3(f)]. This provides a way to control the light propagation by tuning the phase of the magnon squeezing.

Accompanying the MMIT process, the slowing or advancing of light can emerge in this CMM system due to the abnormal dispersion [59–61]. This feature can be characterized by the group delay of the probe light

$$\tau_1=\left.\frac{d\arg(t_p)}{d\xi}\right|_{\xi=\omega_b}. \quad (13)$$

To see this, the corresponding group delay τ_1 is shown in Fig. 4. First, we consider the PMWC case. We have confirmed that MMIT in this CMM system leads only to the

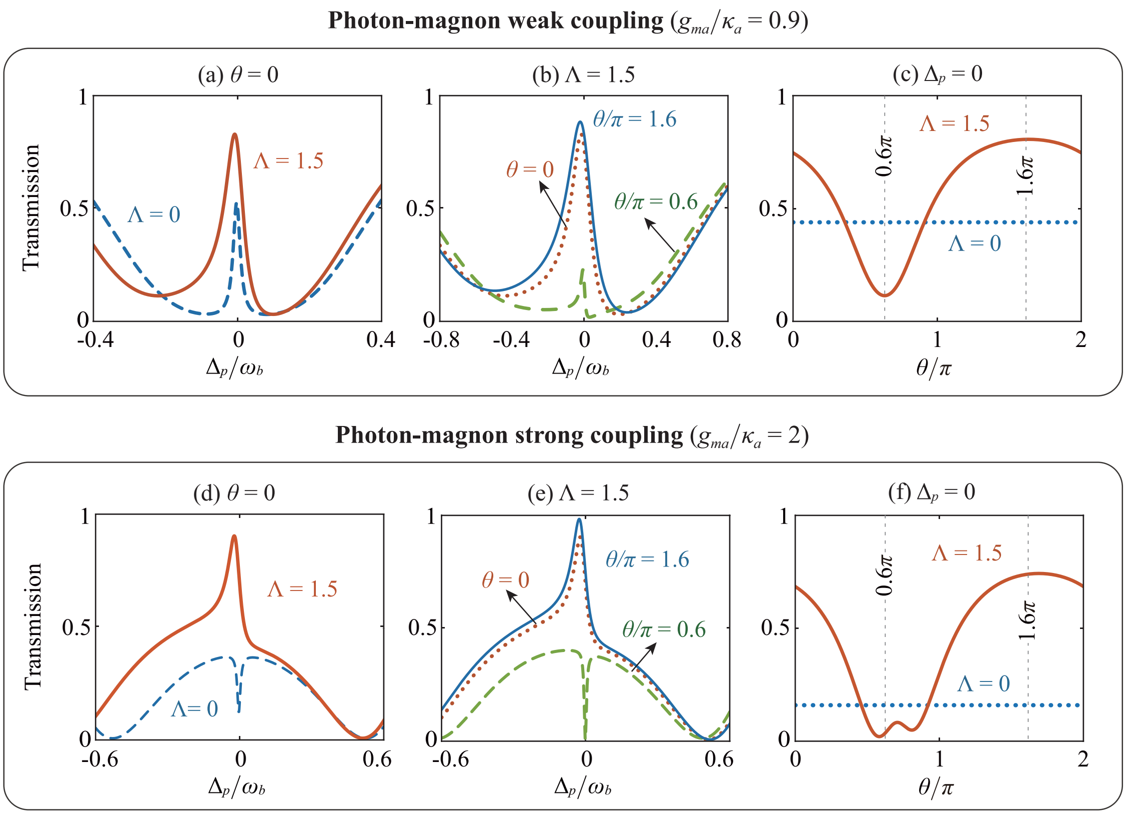

FIG. 3. For the PMWC case ($g_{ma} = 0.9\kappa_a$), the transmission rate of the probe light as a function of the probe detuning $\Delta_p/\omega_b = (\xi - \omega_b)/\omega_b$ (a), (b) and the phase θ (c). For the PMSC case ($g_{ma} = 2\kappa_a$), the transmission rate of the probe light as a function of the probe detuning Δ_p (d), (e) and the phase θ (f). We choose $p_l = 0.5$ W in (a)–(f) and $\Delta_p = 0$ in (c) and (f).

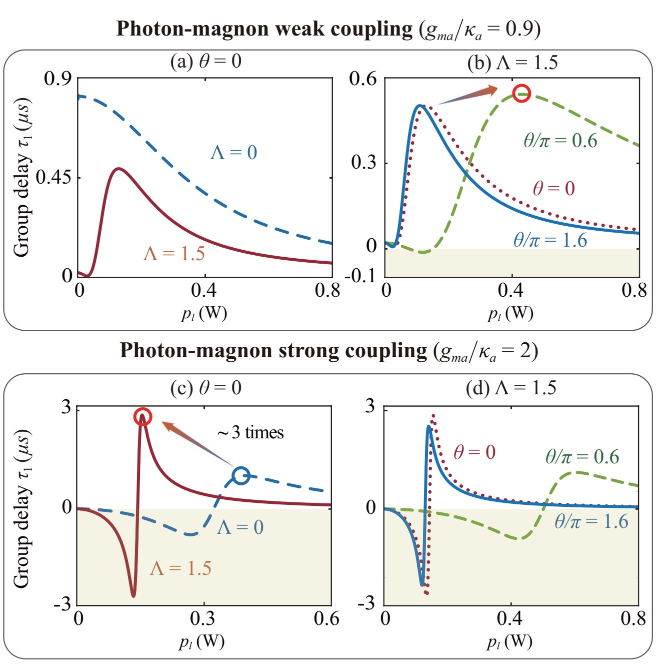

FIG. 4. For the PMWC case ($g_{ma} = 0.9\kappa_a$), group delay of the probe light τ_1 (in the unit of μs) as a function of the drive power p_l with different values (a) Λ and (b) θ. For the PMSC case ($g_{ma} = 2\kappa_a$), group delay of the probe light τ_1 (in the unit of μs) as a function of the drive power p_l with different values (c) Λ and (d) θ. We choose $\theta = 0$ in (a), (c) and $\Lambda = 1.5$ in (b), (d).

slowing of the transmitted light [59–61]. If magnon squeezing is present ($\Lambda = 1.5$ and $\theta = 0$), the group velocity τ_1 tends to decrease compared to the case without the magnon squeezing [see Fig. 3(a)], which is not conducive to storage. Furthermore, we find that the group delay of the probe field τ_1 can be adjusted by controlling the phase θ. For example, the group delay of the probe field τ_1 can be marginally enhanced by tuning the phase θ from 0 or 1.6π to 0.6π [see Fig. 3(b)].

In contrast, for the PMSC case, in the absence of magnon squeezing, the group delay of the probe field τ_1 can be tuned to positive ($\tau_1 \simeq 3$ μs) or negative ($\tau_1 \simeq -3$ μs) by controlling p_l [see the blue dashed curve in Fig. 4(c)]. In particular, if magnon squeezing is present ($\Lambda = 1.5$ and $\theta = 0$), the group delay of the probe field τ_1 can be enhanced by about three times compared to the case without magnon squeezing. In addition, when p_l is kept fixed, one can also drive the system from slow-to-fast or fast-to-slow light regimes by tuning the phase θ [see Fig. 3(d)]. The fact that, in the case of PMSC, the presence of magnon squeezing can strongly modify the dispersion of the CMM system provides a powerful way to enhance slow or fast light by tuning Λ, θ, or p_l, which are not possible in the PMWC scenario. It is well known that slow and fast light effects have been realized in various optomechanical devices [93–96], and slow (fast) light with delay (advance) times up to tens of nanoseconds has been observed and measured. Hence, we confirmed that this effect of magnon squeezing in enhancing slow or fast light and switching from

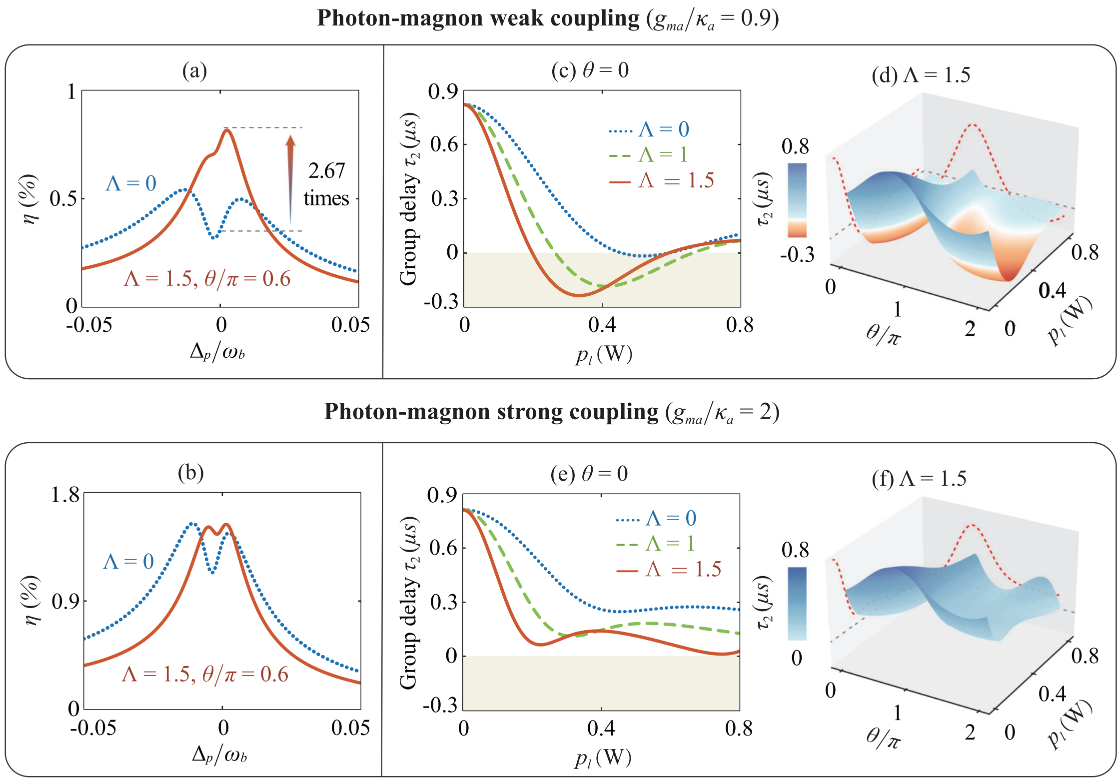

FIG. 5. The efficiency of second-order sideband η as a function of the optical detuning Δ_p with or without ($\Lambda = 0$) magnon squeezing, for (a) PMWC or (b) PMSC. Group delay of second-order sideband τ_2 (in the unit of μs) as a function of the drive power p_l with different Λ, for (c) PMWC or (e) PMSC. Group delay τ_2 (in the unit of μs) as a function of p_l and θ, for (d) PMWC or (f) PMSC. We choose $\Delta_p = 0$ in (c)–(f).

advance to delay of the signal light would be experimentally noticeable.

B. Nonlinear MMIT spectrum and group delay

Now we theoretically study the role of magnon squeezing in further enhancing second-order sidebands in such a CMM system. Figures 5(a) and 4(b) show the efficiency η as a function of Δ_p. For $\Lambda = 0$, the second-order sideband is subdued when the MMIT emerges [59,91], which results in a local minimum between the two sideband peaks around $\Delta_p = 0$ [see the blue dashed curve in Fig. 4(a)]. The efficiency η, which depends on the driving power and the magnon-phonon coupling strength, is extremely small (i.e., 0.2%–0.5%) in the standard CMM system [59]. The reason is that the second-order sideband, which mainly comes from the upconverted first-order sideband, is suppressed due to the enhanced resonance of the anti-Stokes field under the resonance condition [91]. In the PMWC scenario, if magnon squeezing is present (i.e., $\Lambda = 1.5$, $\theta = 0.6\pi$), we find that around the resonance point $\Delta_p = 0$, the second-order sideband is enhanced compared to the standard CMM system (without magnon squeezing) [see Fig. 5(a)], which is helpful for the precise measurement of weak signals [97–99]. For example, the efficiency η is about 0.8% for $\Lambda = 1.5$ and $\theta = 0.6\pi$ at $\Delta_p = 0$, i.e., 2.67 times that for $\Lambda = 0$. This can be explained as follows: Adjusting the squeezing parameter and phase changes the value of $|m_s|^2$, hence the anti-Stokes field is no longer resonantly enhanced when $\theta = 0.6\pi$, and the upconverted process of the first-order sideband is strengthened. In contrast, for the PMSC case, if magnon squeezing is present (i.e., $\Lambda = 1.5$, $\theta = 0.6\pi$), we find that around the resonance point $\Delta_p = 0$, the efficiency η is only marginally enhanced compared to the standard CMM system (without magnon squeezing) [see Fig. 5(b)]. We note that although the magnon squeezing can increase the efficiency of the second-order sideband, this enhancement still only provides an efficiency of 0.8% zero optical detuning, and even less away from zero detuning, and is not observable for the PMSC case. Thus, this effect is not experimentally noticeable. However, we find that the group velocity of the second-order sideband can be adjusted flexibly by utilizing the squeezing of the magnon mode, and this effect can be observed and measured experimentally [93–96]. In the following, we explore the role of magnon squeezing in enhancing the group velocity and switching from advance to delay of the second-order sideband.

The associated group delay of the second-order upper sideband is given by [59–61]

$$\tau_2 = \left.\frac{d\,\arg(\mathcal{A}_2^-)}{2d\xi}\right|_{\xi=\omega_b}, \tag{14}$$

Figures 5(c)–5(f) show the group delay of the second-order sideband τ_2 as a function of the drive power p_l and the phase θ. First, we consider the PMWC case. For $\Lambda = 0$ (without magnon squeezing), with increasing power, slow light always exists [see the blue dotted line in Fig. 5(c)]. However, in the presence of the magnon squeezing, one can tune the group delay of the second-order sideband τ_2 to switch from positive to negative by controlling p_l [see the green dashed line and red solid line in Fig. 5(c)]. Moreover, as Λ increases, the drive power required to convert slow light into fast light decreases. In particular, by controlling the phase θ, the group delay of the second-order sideband is revealed to be capable of switching from fast light to slow light, as shown in Fig. 5(d). Simultaneously, for a fixed p_l, by adjusting the phase to $\theta = 0.6\pi$, the delay time of the second-order sideband can reach the maximum value, which is useful for the storage.

For the PMSC scenario, by tuning Λ, θ, or p_l, the group delay of the second-order signal τ_2 cannot achieve performance similar to the PMWC case, that is, the group velocity cannot be adjusted to be positive or negative [see Figs. 5(e) and 5(f)].

IV. CONCLUSION

In conclusion, we have theoretically studied the features of MMIT in a CMM system with squeezing of the magnon mode. We find that magnon squeezing can strongly affect the magnon number, both in the case of weak or strong photon-magnon coupling. As a result, the transmission rate and the width of the transparency window can be adjusted flexibly by utilizing the squeezing of the magnon mode, and controllable fast-to-slow light switching and and enhancement can be realized. In particular, in the PMSC scenario, the group delay of the probe field can be enhanced by a factor of about 3 due to the presence of magnon squeezing as compared to the case without magnon squeezing, which is not possible in the PMWC scenario. Moreover, in the PMWC scenario, we find that the MMIT second-order sideband can be enhanced, and the group delay of the second-order sideband is revealed to be capable of switching from fast light to slow light by tuning the squeezing parameter and phase, which are not possible in the PMSC scenario. These results indicate that magnon-squeezing-assisted CMM devices can provide a versatile platform to control coherent interactions of photons, phonons, and magnons, for a wide range of potential applications such as microwave-to-optical conversion [24,25], and the sensing of weak forces or magnetic signals [42–44].

ACKNOWLEDGMENTS

H.J. is supported by the National Natural Science Foundation of China (NSFC, Grant No. 11935006) and the Science and Technology Innovation Program of Hunan Province (Grant No. 2020RC4047). T.-X.L. is supported by the NSFC (Grant No. 12205054), the Jiangxi Provincial Education Office Natural Science Fund Project (GJJ211437), and Ph.D. Research Foundation (BSJJ202122). X.X. is supported by the NSFC (Grant No. 12265004).

[1] Z.-L. Xiang, S. Ashhab, J. Q. You, and F. Nori, Hybrid quantum circuits: Superconducting circuits interacting with other quantum systems, Rev. Mod. Phys. **85**, 623 (2013).

[2] D. Lachance-Quirion, Y. Tabuchi, A. Gloppe, K. Usami, and Y. Nakamura, Hybrid quantum systems based on magnonics, Appl. Phys. Express **12**, 070101 (2019).

[3] H. Yuan, Y. Cao, A. Kamra, R. A. Duine, and P. Yan, Quantum magnonics: When magnon spintronics meets quantum information science, Phys. Rep. **965**, 1 (2022).

[4] B. Zare Rameshti, S. Viola Kusminskiy, J. A. Haigh, K. Usami, D. Lachance-Quirion, Y. Nakamura, C.-M. Hu, H. X. Tang, G. E. Bauer, and Y. M. Blanter, Cavity magnonics, Phys. Rep. **979**, 1 (2022).

[5] K. Wang, Y.-P. Gao, R. Jiao, and C. Wang, Recent progress on optomagnetic coupling and optical manipulation based on cavity-optomagnonics, Front. Phys. **17**, 42201 (2022).

[6] Y. Li, W. Zhang, V. Tyberkevych, W.-K. Kwok, A. Hoffmann, and V. Novosad, Hybrid magnonics: Physics, circuits, and applications for coherent information processing, J. Appl. Phys. **128**, 130902 (2020).

[7] Y.-P. Wang and C.-M. Hu, Dissipative couplings in cavity magnonics, J. Appl. Phys. **127**, 130901 (2020).

[8] M. Harder, B. M. Yao, Y. S. Gui, and C.-M. Hu, Coherent and dissipative cavity magnonics, J. Appl. Phys. **129**, 201101 (2021).

[9] H. Huebl, C. W. Zollitsch, J. Lotze, F. Hocke, M. Greifenstein, A. Marx, R. Gross, and S. T. B. Goennenwein, High Cooperativity in Coupled Microwave Resonator Ferrimagnetic Insulator Hybrids, Phys. Rev. Lett. **111**, 127003 (2013).

[10] Y. Tabuchi, S. Ishino, T. Ishikawa, R. Yamazaki, K. Usami, and Y. Nakamura, Hybridizing Ferromagnetic Magnons and Microwave Photons in the Quantum Limit, Phys. Rev. Lett. **113**, 083603 (2014).

[11] X. Zhang, C.-L. Zou, L. Jiang, and H. X. Tang, Strongly Coupled Magnons and Cavity Microwave Photons, Phys. Rev. Lett. **113**, 156401 (2014).

[12] M. Goryachev, W. G. Farr, D. L. Creedon, Y. Fan, M. Kostylev, and M. E. Tobar, High-Cooperativity Cavity QED with Magnons at Microwave Frequencies, Phys. Rev. Appl. **2**, 054002 (2014).

[13] A. Osada, R. Hisatomi, A. Noguchi, Y. Tabuchi, R. Yamazaki, K. Usami, M. Sadgrove, R. Yalla, M. Nomura, and Y. Nakamura, Cavity Optomagnonics with Spin-Orbit Coupled Photons, Phys. Rev. Lett. **116**, 223601 (2016).

[14] X. Zhang, N. Zhu, C.-L. Zou, and H. X. Tang, Optomagnonic Whispering Gallery Microresonators, Phys. Rev. Lett. **117**, 123605 (2016).

[15] J. T. Hou and L. Liu, Strong Coupling between Microwave Photons and Nanomagnet Magnons, Phys. Rev. Lett. **123**, 107702 (2019).

[16] L. Liensberger, A. Kamra, H. Maier-Flaig, S. Geprägs, A. Erb, S. T. B. Goennenwein, R. Gross, W. Belzig, H. Huebl, and M. Weiler, Exchange-Enhanced Ultrastrong Magnon-Magnon Coupling in a Compensated Ferrimagnet, Phys. Rev. Lett. **123**, 117204 (2019).

[17] S. Viola Kusminskiy, H. X. Tang, and F. Marquardt, Coupled spin-light dynamics in cavity optomagnonics, Phys. Rev. A **94**, 033821 (2016).

[18] A. Osada, A. Gloppe, R. Hisatomi, A. Noguchi, R. Yamazaki, M. Nomura, Y. Nakamura, and K. Usami, Brillouin Light Scattering by Magnetic Quasivortices in Cavity Optomagnonics, Phys. Rev. Lett. **120**, 133602 (2018).

[19] J. Xu, C. Zhong, X. Han, D. Jin, L. Jiang, and X. Zhang, Floquet Cavity Electromagnonics, Phys. Rev. Lett. **125**, 237201 (2020).

[20] X. Zhang, C.-L. Zou, N. Zhu, F. Marquardt, L. Jiang, and H. X. Tang, Magnon dark modes and gradient memory, Nat. Commun. **6**, 8914 (2015).

[21] R.-C. Shen, Y.-P. Wang, J. Li, S.-Y. Zhu, G. S. Agarwal, and J. Q. You, Long-Time Memory and Ternary Logic Gate using a Multistable Cavity Magnonic System, Phys. Rev. Lett. **127**, 183202 (2021).

[22] A. V. Chumak, V. I. Vasyuchka, A. A. Serga, and B. Hillebrands, Magnon spintronics, Nat. Phys. **11**, 453 (2015).

[23] L. Bai, M. Harder, P. Hyde, Z. Zhang, C.-M. Hu, Y. P. Chen, and J. Q. Xiao, Cavity Mediated Manipulation of Distant Spin Currents using a Cavity-Magnon-Polariton, Phys. Rev. Lett. **118**, 217201 (2017).

[24] R. Hisatomi, A. Osada, Y. Tabuchi, T. Ishikawa, A. Noguchi, R. Yamazaki, K. Usami, and Y. Nakamura, Bidirectional conversion between microwave and light via ferromagnetic magnons, Phys. Rev. B **93**, 174427 (2016).

[25] Y. S. Ihn, S.-Y. Lee, D. Kim, S. H. Yim, and Z. Kim, Coherent multimode conversion from microwave to optical wave via a magnon-cavity hybrid system, Phys. Rev. B **102**, 064418 (2020).

[26] C.-Z. Chai, Z. Shen, Y.-L. Zhang, H.-Q. Zhao, G.-C. Guo, C.-L. Zou, and C.-H. Dong, Single-sideband microwave-to-optical conversion in high-Q ferrimagnetic microspheres, Photon. Res. **10**, 820 (2022).

[27] D. Zhang, X.-Q. Luo, Y.-P. Wang, T.-F. Li, and J. Q. You, Observation of the exceptional point in cavity magnon-polaritons, Nat. Commun. **8**, 1368 (2017).

[28] M. Harder, L. Bai, P. Hyde, and C.-M. Hu, Topological properties of a coupled spin-photon system induced by damping, Phys. Rev. B **95**, 214411 (2017).

[29] B. Wang, Z.-X. Liu, C. Kong, H. Xiong, and Y. Wu, Magnon-induced transparency and amplification in $\mathcal{PT}$-symmetric cavity-magnon system, Opt. Express **26**, 20248 (2018).

[30] G.-Q. Zhang and J. Q. You, Higher-order exceptional point in a cavity magnonics system, Phys. Rev. B **99**, 054404 (2019).

[31] X. Zhang, K. Ding, X. Zhou, J. Xu, and D. Jin, Experimental Observation of an Exceptional Surface in Synthetic Dimensions with Magnon Polaritons, Phys. Rev. Lett. **123**, 237202 (2019).

[32] Y. Cao and P. Yan, Exceptional magnetic sensitivity of $\mathscr{PT}$-symmetric cavity magnon polaritons, Phys. Rev. B **99**, 214415 (2019).

[33] M. Harder, Y. Yang, B. M. Yao, C. H. Yu, J. W. Rao, Y. S. Gui, R. L. Stamps, and C.-M. Hu, Level Attraction Due to Dissipative Magnon-Photon Coupling, Phys. Rev. Lett. **121**, 137203 (2018).

[34] P.-C. Xu, J. W. Rao, Y. S. Gui, X. Jin, and C.-M. Hu, Cavity-mediated dissipative coupling of distant magnetic moments: Theory and experiment, Phys. Rev. B **100**, 094415 (2019).

[35] H. Y. Yuan, P. Yan, S. Zheng, Q. Y. He, K. Xia, and M.-H. Yung, Steady Bell State Generation via Magnon-Photon Coupling, Phys. Rev. Lett. **124**, 053602 (2020).

[36] J. Zhao, Y. Liu, L. Wu, C.-K. Duan, Y.-X. Liu, and J. Du, Observation of Anti-$\mathscr{PT}$-Symmetry Phase Transition in the Magnon-Cavity-Magnon Coupled System, Phys. Rev. Appl. **13**, 014053 (2020).

[37] Y. Yang, Y.-P. Wang, J. W. Rao, Y. S. Gui, B. M. Yao, W. Lu, and C.-M. Hu, Unconventional Singularity in Anti-Parity-Time Symmetric Cavity Magnonics, Phys. Rev. Lett. **125**, 147202 (2020).

[38] Z. Zhang, M. O. Scully, and G. S. Agarwal, Quantum entanglement between two magnon modes via Kerr nonlinearity driven far from equilibrium, Phys. Rev. Res. **1**, 023021 (2019).

[39] J. M. P. Nair and G. S. Agarwal, Deterministic quantum entanglement between macroscopic ferrite samples, Appl. Phys. Lett. **117**, 084001 (2020).

[40] Y.-P. Wang, J. W. Rao, Y. Yang, P.-C. Xu, Y. S. Gui, B. M. Yao, J. Q. You, and C.-M. Hu, Nonreciprocity and Unidirectional Invisibility in Cavity Magnonics, Phys. Rev. Lett. **123**, 127202 (2019).

[41] Y. T. Zhao, J. W. Rao, Y. S. Gui, Y. P. Wang, and C.-M. Hu, Broadband Nonreciprocity Realized by Locally Controlling the Magnon's Radiation, Phys. Rev. Appl. **14**, 014035 (2020).

[42] T. Trickle, Z. Zhang, and K. M. Zurek, Detecting Light Dark Matter with Magnons, Phys. Rev. Lett. **124**, 201801 (2020).

[43] S. P. Wolski, D. Lachance-Quirion, Y. Tabuchi, S. Kono, A. Noguchi, K. Usami, and Y. Nakamura, Dissipation-Based Quantum Sensing of Magnons with a Superconducting Qubit, Phys. Rev. Lett. **125**, 117701 (2020).

[44] M. S. Ebrahimi, A. Motazedifard, and M. B. Harouni, Single-quadrature quantum magnetometry in cavity electromagnonics, Phys. Rev. A **103**, 062605 (2021).

[45] D. Lachance-Quirion, S. Piotr Wolski, Y. Tabuchi, S. Kono, K. Usami, and Y. Nakamura, Entanglement-based single-shot detection of a single magnon with a superconducting qubit, Science **367**, 425 (2020).

[46] X. Zhang, C. L. Zou, L. Jiang, and H. X. Tang, Cavity magnomechanics, Sci. Adv. **2**, e1501286 (2016).

[47] C. A. Potts, E. Varga, V. A. S. V. Bittencourt, S. V. Kusminskiy, and J. P. Davis, Dynamical Backaction Magnomechanics, Phys. Rev. X **11**, 031053 (2021).

[48] R.-C. Shen, J. Li, Z.-Y. Fan, Y.-P. Wang, and J. Q. You, Mechanical Bistability in Kerr-modified Cavity Magnomechanics, Phys. Rev. Lett. **129**, 123601 (2022).

[49] Z. Shen, G.-T. Xu, M. Zhang, Y.-L. Zhang, Y. Wang, C.-Z. Chai, C.-L. Zou, G.-C. Guo, and C.-H. Dong, Coherent Coupling between Phonons, Magnons, and Photons, Phys. Rev. Lett. **129**, 243601 (2022).

[50] J. Li, S.-Y. Zhu, and G. S. Agarwal, Magnon-Photon-Phonon Entanglement in Cavity Magnomechanics, Phys. Rev. Lett. **121**, 203601 (2018).

[51] J. Li and S.-Y. Zhu, Entangling two magnon modes via magnetostrictive interaction, New J. Phys. **21**, 085001 (2019).

[52] M. Yu, H. Shen, and J. Li, Magnetostrictively Induced Stationary Entanglement between Two Microwave Fields, Phys. Rev. Lett. **124**, 213604 (2020).

[53] Z.-Y. Fan, L. Qiu, S. Gröblacher, and J. Li, Microwave-optics entanglement via cavity optomagnomechanics, arXiv:2208.10703.

[54] J. Li and S. Gröblacher, Entangling the vibrational modes of two massive ferromagnetic spheres using cavity magnomechanics, Quantum Sci. Technol. **6**, 024005 (2021).

[55] Y.-T. Chen, L. Du, Y. Zhang, and J.-H. Wu, Perfect transfer of enhanced entanglement and asymmetric steering in a cavity-magnomechanical system, Phys. Rev. A **103**, 053712 (2021).

[56] M.-S. Ding, X.-X. Xin, S.-Y. Qin, and C. Li, Enhanced entanglement and steering in $\mathscr{PT}$-symmetric cavity magnomechanics, Opt. Commun. **490**, 126903 (2021).

[57] J. Li, S.-Y. Zhu, and G. S. Agarwal, Squeezed states of magnons and phonons in cavity magnomechanics, Phys. Rev. A **99**, 021801(R) (2019).
[58] W. Zhang, D.-Y. Wang, C.-H. Bai, T. Wang, S. Zhang, and H.-F. Wang, Generation and transfer of squeezed states in a cavity magnomechanical system by two-tone microwave fields, Opt. Express **29**, 11773 (2021).
[59] S.-N. Huai, Y.-L. Liu, J. Zhang, L. Yang, and Y.-X. Liu, Enhanced sideband responses in a $\mathcal{PT}$-symmetric-like cavity magnomechanical system, Phys. Rev. A **99**, 043803 (2019).
[60] C. Kong, B. Wang, Z.-X. Liu, H. Xiong, and Y. Wu, Magnetically controllable slow light based on magnetostrictive forces, Opt. Express **27**, 5544 (2019).
[61] K. Ullah, M. T. Naseem, and O. E. Müstecaplıoğlu, Tunable multiwindow magnomechanically induced transparency, Fano resonances, and slow-to-fast light conversion, Phys. Rev. A **102**, 033721 (2020).
[62] B. Wang, X. Jia, X.-H. Lu, and H. Xiong, $\mathcal{PT}$-symmetric magnon laser in cavity optomagnonics, Phys. Rev. A **105**, 053705 (2022).
[63] Z.-X. Liu and H. Xiong, Magnon laser based on Brillouin light scattering, Opt. Lett. **45**, 5452 (2020).
[64] M. Wang, D. Zhang, X.-H. Li, Y.-Y. Wu, and Z.-Y. Sun, Magnon chaos in $\mathcal{PT}$-symmetric cavity magnomechanics, IEEE Photon. J. **11**, 5300108 (2019).
[65] M. F. Colombano, G. Arregui, F. Bonell, N. E. Capuj, E. Chavez-Angel, A. Pitanti, S. O. Valenzuela, C. M. Sotomayor-Torres, D. Navarro-Urrios, and M. V. Costache, Ferromagnetic Resonance Assisted Optomechanical Magnetometer, Phys. Rev. Lett. **125**, 147201 (2020).
[66] C. A. Potts, V. A. S. V. Bittencourt, S. V. Kusminskiy, and J. P. Davis, Magnon-Phonon Quantum Correlation Thermometry, Phys. Rev. Appl. **13**, 064001 (2020).
[67] A. Kani, B. Sarma, and J. Twamley, Intensive Cavity-Magnomechanical Cooling of a Levitated Macromagnet, Phys. Rev. Lett. **128**, 013602 (2022).
[68] M.-S. Ding, L. Zheng, and C. Li, Ground-state cooling of a magnomechanical resonator induced by magnetic damping, J. Opt. Soc. Am. B **37**, 627 (2020).
[69] Z.-X. Yang, L. Wang, Y.-M. Liu, D.-Y. Wang, C.-H. Bai, S. Zhang, and H.-F. Wang, Ground state cooling of magnomechanical resonator in $\mathcal{PT}$-symmetric cavity magnomechanical system at room temperature, Front. Phys. **15**, 52504 (2020).
[70] T.-X. Lu, H. Zhang, Q. Zhang, and H. Jing, Exceptional-point-engineered cavity magnomechanics, Phys. Rev. A **103**, 063708 (2021).
[71] S.-f. Qi and J. Jing, Magnon-assisted photon-phonon conversion in the presence of structured environments, Phys. Rev. A **103**, 043704 (2021).
[72] S.-f. Qi and J. Jing, Accelerated adiabatic passage in cavity magnomechanics, Phys. Rev. A **105**, 053710 (2022).
[73] B. Sarma, T. Busch, and J. Twamley, Cavity magnomechanical storage and retrieval of quantum states, New J. Phys. **23**, 043041 (2021).
[74] M. Asjad, J. Li, S.-Y. Zhu, and J. You, Magnon squeezing enhanced ground-state cooling in cavity magnomechanics, Fundam. Res. **3**, 3 (2023).
[75] M.-S. Ding, L. Zheng, Y. Shi, and Y.-J. Liu, Magnon squeezing enhanced entanglement in a cavity magnomechanical system, J. Opt. Soc. Am. B **39**, 2665 (2022).
[76] S. L. Braunstein and P. van Loock, Quantum information with continuous variables, Rev. Mod. Phys. **77**, 513 (2005).
[77] A. Abramovici, W. E. Althouse, R. W. P. Drever, Y. Gürsel, S. Kawamura, F. J. Raab, D. Shoemaker, L. Sievers, R. E. Spero, K. S. Thorne, R. E. Vogt, R. Weiss, S. E. Whitcomb, and M. E. Zucker, LIGO: The laser interferometer gravitational-wave observatory, Science **256**, 325 (1992).
[78] W. Zhao, S.-D. Zhang, A. Miranowicz, and H. Jing, Weak-force sensing with squeezed optomechanics, Sci. China: Phys. Mech. Astron. **63**, 224211 (2020).
[79] A. Furusawa, J. L. Sørensen, S. L. Braunstein, C. A. Fuchs, H. J. Kimble, and E. S. Polzik, Unconditional quantum teleportation, Science **282**, 706 (1998).
[80] S. Haroche, Nobel lecture: Controlling photons in a box and exploring the quantum to classical boundary, Rev. Mod. Phys. **85**, 1083 (2013).
[81] M. F. Bocko and R. Onofrio, On the measurement of a weak classical force coupled to a harmonic oscillator: Experimental progress, Rev. Mod. Phys. **68**, 755 (1996).
[82] A. Bienfait, P. Campagne-Ibarcq, A. H. Kiilerich, X. Zhou, S. Probst, J. J. Pla, T. Schenkel, D. Vion, D. Esteve, J. J. L. Morton, K. Moelmer, and P. Bertet, Magnetic Resonance with Squeezed Microwaves, Phys. Rev. X **7**, 041011 (2017).
[83] M. Peng, H. Zhang, Q. Zhang, T.-X. Lu, I. M. Mirza, and H. Jing, Nonreciprocal slow or fast light in anti-$\mathcal{PT}$-symmetric optomechanics, Phys. Rev. A **107**, 033507 (2023).
[84] A. Kamra and W. Belzig, Super-Poissonian Shot Noise of Squeezed-Magnon Mediated Spin Transport, Phys. Rev. Lett. **116**, 146601 (2016).
[85] J. Li, Y.-P. Wang, J.-Q. You, and S.-Y. Zhu, Squeezing microwaves by magnetostriction, Natl. Sci. Rev. **10**, nwac247 (2022).
[86] Q. Guo, D. Xu, J. Cheng, H. Tan, and J. Li, Magnon squeezing by two-tone driving of a qubit in cavity-magnon-qubit systems, arXiv:2304.10760.
[87] S. Weis, R. Rivière, S. Deléglise, E. Gavartin, O. Arcizet, A. Schliesser, and T. J. Kippenberg, Optomechanically induced transparency, Science **330**, 1520 (2010).
[88] T.-X. Lu, Y.-F. Jiao, H.-L. Zhang, F. Saif, and H. Jing, Selective and switchable optical amplification with mechanical driven oscillators, Phys. Rev. A **100**, 013813 (2019).
[89] H. Lü, C. Wang, L. Yang, and H. Jing, Optomechanically Induced Transparency at Exceptional Points, Phys. Rev. Appl. **10**, 014006 (2018).
[90] C. Fabre, M. Pinard, S. Bourzeix, A. Heidmann, E. Giacobino, and S. Reynaud, Quantum-noise reduction using a cavity with a movable mirror, Phys. Rev. A **49**, 1337 (1994).
[91] H. Xiong, L.-G. Si, A.-S. Zheng, X. Yang, and Y. Wu, Higher-order sidebands in optomechanically induced transparency, Phys. Rev. A **86**, 013815 (2012).
[92] C. W. Gardiner and M. J. Collett, Input and output in damped quantum systems: Quantum stochastic differential equations and the master equation, Phys. Rev. A **31**, 3761 (1985).
[93] A. H. Safavi-Naeini, T. P. M. Alegre, J. Chan, M. Eichenfield, M. Winger, Q. Lin, J. T. Hill, D. E. Chang, and O. Painter, Electromagnetically induced transparency and slow light with optomechanics, Nature (London) **472**, 69 (2011).

[94] V. Fiore, Y. Yang, M. C. Kuzyk, R. Barbour, L. Tian, and H. Wang, Storing Optical Information as a Mechanical Excitation in a Silica Optomechanical Resonator, Phys. Rev. Lett. **107**, 133601 (2011).

[95] V. Fiore, C. Dong, M. C. Kuzyk, and H. Wang, Optomechanical light storage in a silica microresonator, Phys. Rev. A **87**, 023812 (2013).

[96] X. Zhou, F. Hocke, A. Schliesser, A. Marx, H. Huebl, R. Gross, and T. J. Kippenberg, Slowing, advancing and switching of microwave signals using circuit nanoelectromechanics, Nat. Phys. **9**, 179 (2013).

[97] H. Xiong, Z.-X. Liu, and Y. Wu, Highly sensitive optical sensor for precision measurement of electrical charges based on optomechanically induced difference-sideband generation, Opt. Lett. **42**, 3630 (2017).

[98] C. Kong, H. Xiong, and Y. Wu, Coulomb-interaction-dependent effect of high-order sideband generation in an optomechanical system, Phys. Rev. A **95**, 033820 (2017).

[99] Z.-X. Liu, B. Wang, C. Kong, L.-G. Si, H. Xiong, and Y. Wu, A proposed method to measure weak magnetic field based on a hybrid optomechanical system, Sci. Rep. **7**, 12521 (2017).